



## Short communication

MoS<sub>2</sub> cleaning by acetone and UV-ozone: Geological and synthetic material

Keren M. Freedy<sup>a</sup>, Maria Gabriela Sales<sup>a</sup>, Peter M. Litwin<sup>a</sup>, Sergiy Krylyuk<sup>b,c</sup>, Pranab Mohapatra<sup>d</sup>, Ariel Ismach<sup>d</sup>, Albert V. Davydov<sup>c</sup>, Stephen J. McDonnell<sup>a,\*</sup>

<sup>a</sup> Department of Materials Science and Engineering, University of Virginia, Charlottesville, VA 22904, United States of America

<sup>b</sup> Theiss Research, Inc., La Jolla, CA 92037, United States of America

<sup>c</sup> Materials Science and Engineering Division, National Institute of Standards and Technology (NIST), Gaithersburg, MD 20899, United States of America

<sup>d</sup> Department of Materials Science and Engineering, Tel Aviv University, Ramat Aviv, Tel Aviv, 6997801, Israel



## ARTICLE INFO

## Keywords:

Surface treatments  
Ozone  
X-ray photoelectron spectroscopy  
Photoresist residues

## ABSTRACT

The effects of poly(methyl methacrylate) PMMA removal procedures on the surface chemistry of both geological and synthetic MoS<sub>2</sub> are investigated. X-ray photoelectron spectroscopy (XPS) is employed following acetone dissolution, thermal annealing, and ultraviolet-ozone (UV-O<sub>3</sub>) treatment of PMMA-coated MoS<sub>2</sub> samples. Specifically, we focus on the efficacy of polymer residue removal procedures and oxidation resistance of the different samples. Acetone dissolution followed by ultra-high vacuum (UHV) annealing was highly effective in removing carbon residues from one type of geological sample however not for a synthetic sample produced by sulfurization. Similarly, different types of samples require varying lengths of UV-O<sub>3</sub> exposure time for proper removal of residues, and some exhibit oxidation as a result. UV-O<sub>3</sub> exposure followed by a UHV anneal resulted in successful removal of carbon residues from MoS<sub>2</sub> produced by sulfurization while a substantial carbon signal remained on a chemical vapor deposited MoS<sub>2</sub> sample subjected to the same process. Differences in the effects of removal procedures are attributed to differences in surface morphology and material quality. For device fabrication applications, this work highlights the importance of developing PMMA removal processes specific to the MoS<sub>2</sub> used with full consideration for the processing required to obtain the MoS<sub>2</sub>.

Poly(methyl methacrylate) (PMMA) is commonly used for the transfer and photolithographic processing of 2D materials [1]. Chemical dissolution of PMMA in acetone is known to leave polymer residues on the surface of the sample [2–4]. In graphene-based devices, the presence of PMMA residues has been found to significantly affect important device properties such as doping, mobility, and contact resistance [5–9]. Contamination from polymer residues can also result in non-conformal growth of gate dielectric layers [10]. To decompose the residues following PMMA dissolution in acetone, the sample is typically annealed in vacuum or a controlled gas environment. Exposure to ultraviolet-ozone (UV-O<sub>3</sub>) has also been suggested to aid in the removal of PMMA residues, manifesting in reduced contact resistance in graphene devices [7,9]. While the removal of residues from graphene has been studied extensively, the effects of PMMA residues and means of their removal from MoS<sub>2</sub> are not reported to date. This work uses X-ray photoelectron spectroscopy (XPS) to characterize MoS<sub>2</sub> following different PMMA removal procedures, including acetone dissolution, UV-O<sub>3</sub> treatment, thermal annealing in ultra-high vacuum (UHV), and a combination of the three processes.

UV-O<sub>3</sub> treatment of MoS<sub>2</sub> has been previously implemented for a

variety of applications in film growth and device processing on MoS<sub>2</sub> materials of different types. For example, Azcatl et al. use UV-O<sub>3</sub> to functionalize the surface of mechanically exfoliated geological MoS<sub>2</sub> for improved atomic layer deposition of gate dielectrics [11,12] and Van Le et al. demonstrate improved performance of photovoltaics with UV-O<sub>3</sub> treatment of MoS<sub>2</sub> nanosheets derived from sonication of MoS<sub>2</sub> powder [13]. Evidence suggests that different types of MoS<sub>2</sub> material can exhibit differences in surface chemistry upon UV-O<sub>3</sub> exposure. For example, Azcatl et al. [11] show that geological MoS<sub>2</sub> exposed to UV-O<sub>3</sub> for 15 min does not form Mo oxide nor exhibit MoS<sub>2</sub> bond scission, whereas Yang et al. [14] and Van Le et al. [13] observe oxidation of MoS<sub>2</sub> monolayer nanosheets after 3 min and 15 min of UV-O<sub>3</sub> treatment, respectively. Park et al. [15] demonstrate that the formation of oxide is dependent on UV-O<sub>3</sub> power settings. Power settings are scarcely reported meaning that results from independent studies in the literature cannot be compared in an attempt to discern differences between different types of MoS<sub>2</sub>. Understanding potential differences requires a side-by-side comparison of samples processed with identical parameters. This was performed by Kurabayashi et al. [16], who report that geological MoS<sub>2</sub> has a higher oxidation resistance to UV-O<sub>3</sub> than

\* Corresponding author.

E-mail address: [mcdonnell@virginia.edu](mailto:mcdonnell@virginia.edu) (S.J. McDonnell).

chemical vapor deposited (CVD) material. Nevertheless, the effect of UV-O<sub>3</sub> treatment on polymer removal from geological and synthetic MoS<sub>2</sub> is not yet reported. Our work examines UV-O<sub>3</sub> for polymer removal from synthesized films and bulk geological MoS<sub>2</sub> crystals, both of which are frequently used for device fabrication.

Two types of synthetic material were examined in this study. The first synthetic MoS<sub>2</sub> was synthesized by sulfurizing thin Mo films. This method is similar to that of Tarasov et al. [17]. Mo films 4 nm thick were e-beam deposited onto SiO<sub>2</sub>/Si substrates that were cleaned with acetone, isopropanol and de-ionized water. The substrates were loaded into a home-built horizontal CVD reactor and sulfurized at 750 °C and 1.6 kPa for 20 min using 30 sccm (standard cm<sup>3</sup>/min) flow of H<sub>2</sub>S diluted with 1000 sccm Ar carrier gas. This method produced ≈ 10 nm thick polycrystalline MoS<sub>2</sub> films with an average grain size of ≈ 20 nm. The second type of synthetic sample, CVD MoS<sub>2</sub>, was synthesized using a micro-cavity based CVD technique at atmospheric pressure while flowing ultrahigh pure Ar gas. MoO<sub>3</sub> and sulfur powders were evaporated at 750 °C onto a sapphire substrate sonicated in acetone and isopropanol [18]. The MoS<sub>2</sub> films were transferred to a SiO<sub>2</sub>/Si substrate following reported procedures using a polystyrene film [19]. Additional details of the growth and transfer processes are included in Supporting information. Geological MoS<sub>2</sub> samples from two different vendors (SPI [20] and Ward Science [21]<sup>1</sup>) were investigated in addition to the synthetic samples. Bulk geological crystals were mechanically exfoliated for surface cleaning immediately prior to PMMA spin coating.

Both types of synthetic and geological MoS<sub>2</sub> samples were spin coated with a 30 mg/mL solution of PMMA (M<sub>w</sub> ≈ 996,000 by GPC) in chlorobenzene at 3000 rpm for 1 min and then 1000 rpm for 1 min with an acceleration rate of 1000 rpm/s [5]. After spin coating, the samples were left on a hot plate for 10 min at 60 °C to cure the PMMA. The samples were then soaked in acetone for 2 h and subsequently treated under different conditions before XPS characterization. UV-O<sub>3</sub> treatment was performed in air using a UV grid lamp connected to a 3 kV, 0.03 A power supply (BHK, Inc.). XPS data was acquired using two different systems. Experiments 1 and 2 described in Table 1 were performed with a Scienta R3000 analyzer at a pass energy of 50 eV with a monochromated Al Kα X-ray source in a Scienta-Omicron UHV system described elsewhere [22]. Experiment 3 described in Table 1 was performed in a PHI VersaProbe III UHV system with a monochromated Al Kα X-ray source at a pass energy of 26 eV and a spot size of 100 μm. Annealing was performed in the same UHV chamber as the XPS, meaning that the samples were not exposed to air after the final annealing step.

Fig. 1(a) shows the C 1s spectra for both samples after PMMA dissolution in acetone and after annealing in UHV at 550 °C for 30 min (Experiment 1). The carbon on the starting material is adventitious carbon with a primary component at about 284 eV corresponding to C–C bonds and higher binding energy components corresponding to C–O–C and C–OH bonds [23]. After spin coating, curing, and dissolving PMMA in acetone, the total carbon signal increased by approximately a factor of 2 in the Synthetic A sample and by a factor of 5 in the Geological A sample. These numbers indicate a substantial quantity of PMMA residues when compared with adventitious carbon. It is not surprising that less adventitious carbon was present on the starting surface of the geological sample since it was exfoliated immediately prior to the experiment. There is also less PMMA residue left on the geological sample. This might be explained by the fact that the two samples exhibit drastically different surface morphologies as shown in

**Table 1**  
Experiment processes.

	Process	Samples
Experiment 1	PMMA spin-coating 2 h removal in acetone 30 min UHV anneal at 550 °C	Synthetic A (sulfurized Mo) Geological A (SPI)
Experiment 2	PMMA spin-coating 2 h removal in acetone Sequential UV-O <sub>3</sub> exposures 30 min UHV anneal at 550 °C	Synthetic A (sulfurized Mo) Geological A (SPI)
Experiment 3	PMMA spin-coating 2 h removal in acetone 2 min UV-O <sub>3</sub> exposures 30 min UHV anneal at 550 °C	Synthetic A (sulfurized Mo) Synthetic B (CVD) Geological A (SPI) Geological B (Ward's)

the atomic force microscopy (AFM) images in Fig. 2. The root-mean-square (RMS) surface roughness of the Synthetic A sample was found to be 1.7 nm (Fig. 2(a)) whereas the Geological A sample has a surface roughness of 73 pm (Fig. 2(b)) in agreement with literature values [24], indicating that it is atomically flat. Higher surface roughness in the synthetic sample also provides more surface area for PMMA residues to physisorb. We also note the emergence of a state at ≈ 290 eV corresponding to C=O bonds [25,26] which disappears after annealing. Following annealing, 30% of the acetone-dissolved PMMA carbon signal remains on the Synthetic A sample whereas only 9% remains on the Geological A sample. It is clear that annealing after solvent dissolution of PMMA is not sufficient for achieving a clean MoS<sub>2</sub> surface. As Fig. 1(b) indicates, no significant changes in the Mo 3d and S 2p regions are observed in the Synthetic A sample. We note that after annealing there is an asymmetry on the low binding energy side of the Mo and S regions of the geological sample. This is likely due to the variations in local doping typical of geological samples [27].

To determine if UV-O<sub>3</sub> treatment prior to UHV annealing can enhance the removal of carbon, a second set of samples were sequentially exposed to UV-O<sub>3</sub> for varying lengths of time after an initial PMMA dissolution with acetone (Experiment 2). These samples were measured with XPS after each treatment. The carbon spectra for synthetic and geological samples after UV-O<sub>3</sub> treatment are shown in Fig. 3(a). Air exposure between treatments led to a slight increase in the carbon signal of the geological sample between the 0.5 min and 1 min treatments, however the general trend for both samples is a steady reduction in the carbon signal with increasing UV-O<sub>3</sub> exposure time. All carbon is removed from the surface of the synthetic sample after a total of 10 min and from the geological sample after 5 min.

Spectral changes are observed in the Mo 3d and S 2p regions, shown in Fig. 3(b), indicating modifications in the surface chemistry of the material as a result of UV-O<sub>3</sub> and post-treatment annealing. In the Synthetic A sample, we detect the increase of the Mo–O state after 2 min of exposure. The state increases in intensity relative to the Mo–S state as UV-O<sub>3</sub> exposure time is increased. After 10 min of exposure, 50% of the Mo signal corresponds to Mo–O. In contrast, no Mo–O is observed in the Geological A sample at any time meaning that Mo–S bonds are preserved. The RSF-normalized S/Mo ratio of the Mo–S state stays constant at a value of approximately 2 for all exposure times for both samples.

In the S 2p spectrum, we begin to see a new doublet after 5 min in the Synthetic A sample and after 2 min in the Geological A sample at a binding energy of ≈ 164.8 eV. This state was also reported by Azcatl et al. [11] in a geological MoS<sub>2</sub> sample without any evidence of Mo–S bond scission, and is therefore thought to correspond to S–O bonds from oxygen adsorbed to rehybridized sulfur atoms on the surface of the material. The appearance of this state in our geological sample, which also does not exhibit Mo–S bond scission, is consistent with this assignment. In the Synthetic A sample, we begin to observe the S<sup>6+</sup> oxidation state at ≈ 168 eV [28] after 5 min, indicating the presence of SO<sub>x</sub>. The formation of sulfur oxide in the film is not surprising given the

<sup>1</sup> Certain commercial equipment instruments or materials are identified in this paper to foster understanding. Such identification does not imply recommendation or endorsement by the National Institute of Standards and Technology nor does it imply that the materials or equipment identified are necessarily the best available for the purpose.

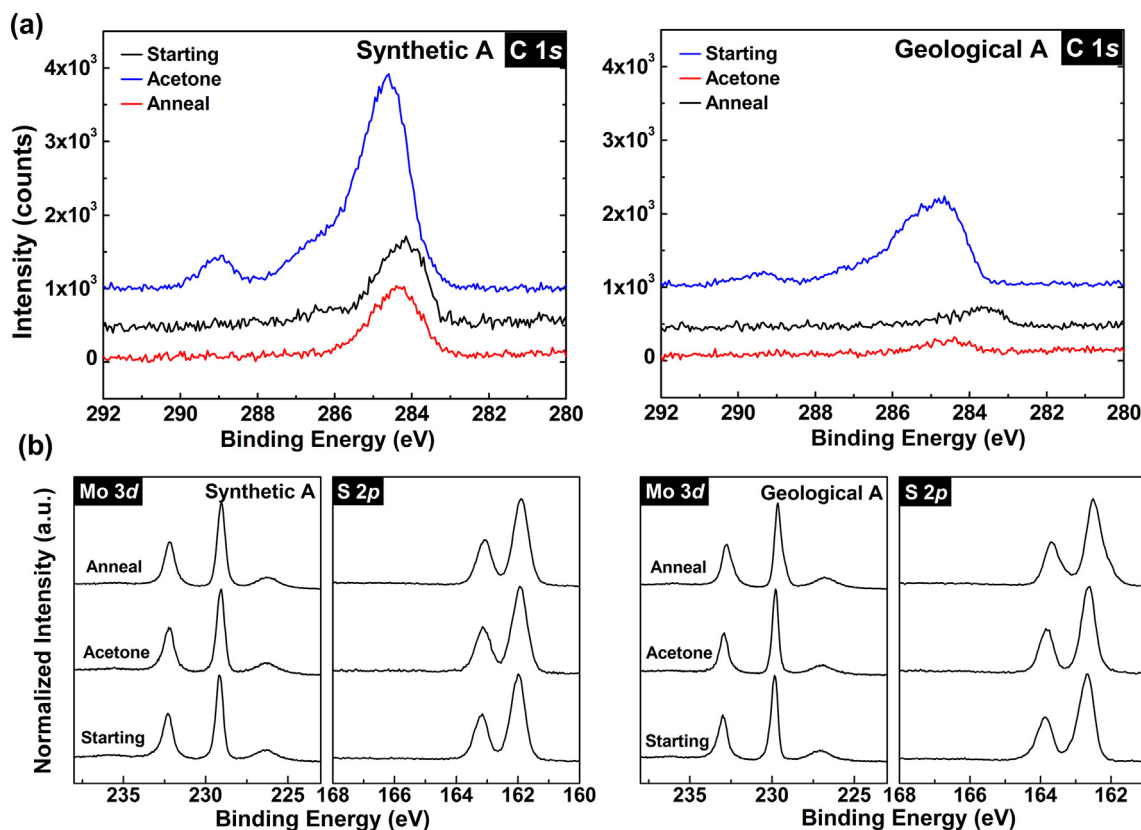


Fig. 1. (a) C 1s, (b) Mo 3d and S 2p spectra acquired on starting material, after acetone dissolution, and after UHV annealing.

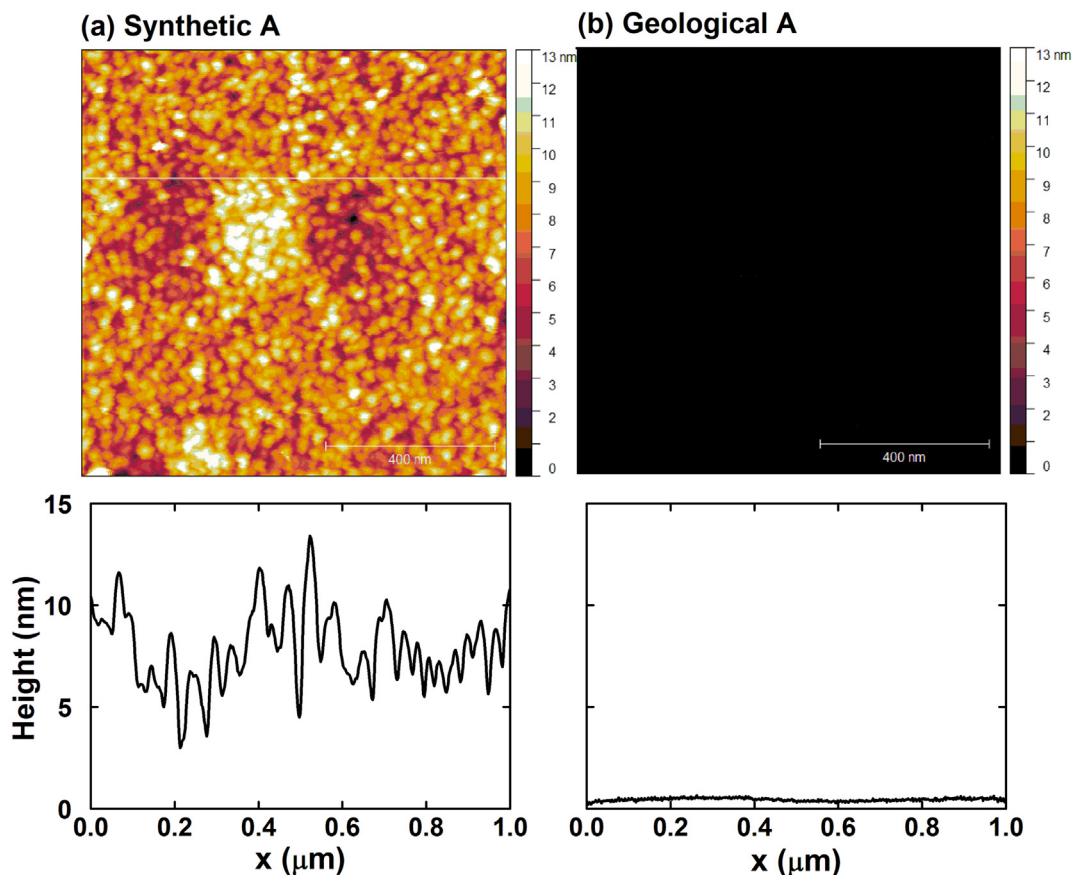


Fig. 2. AFM images of (a) sulfurized MoS<sub>2</sub> and (b) geological material showing a drastic difference in surface roughness.

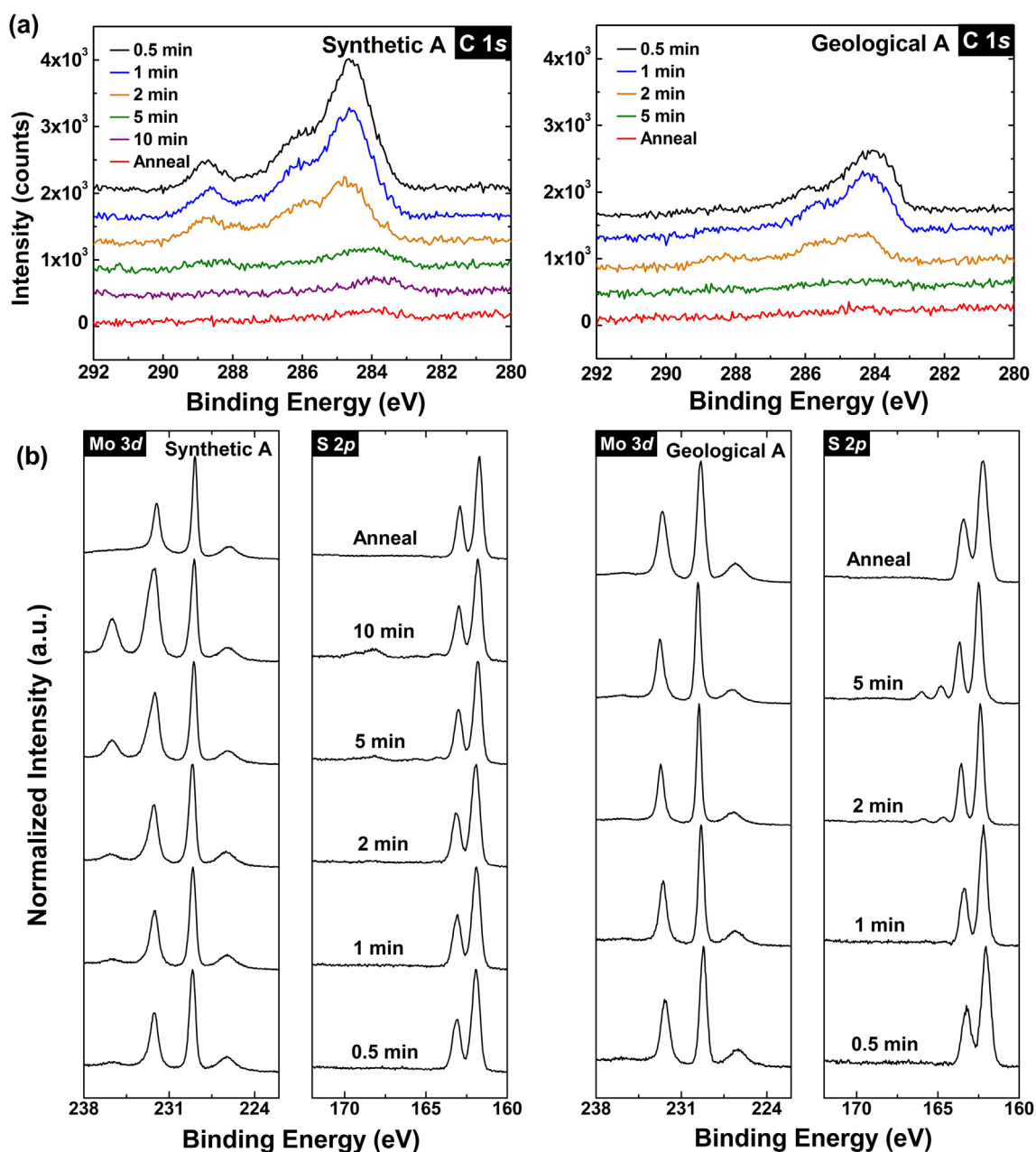


Fig. 3. (a) C 1s, (b) Mo 3d and S 2p spectra acquired after varying lengths of UV-O<sub>3</sub> exposure time.

formation of MoO<sub>x</sub>, which is indicative of Mo–S bond scission. Synthetic MoS<sub>2</sub> is known to have inferior crystalline quality (i.e., higher density of defects) compared to geological materials [29]. This explains its susceptibility to damage by UV-O<sub>3</sub> in comparison to the geological sample. After UV-O<sub>3</sub>, the samples were annealed in UHV at 550 °C resulting in some removal of oxide states. In both samples, the surface-bonded oxygen was thermally desorbed, and no change in S/Mo stoichiometry was observed. While the MoS<sub>2</sub> chemistry is comparable to its initial condition, the effects of UV-O<sub>3</sub> damage on the electronic properties of the material are not examined here. The oxidation behavior of the Synthetic A sample is discussed in Supporting information.

We note that the samples used in Experiments 1 and 2 are not a comprehensive sampling of the wide variety geological and synthetic MoS<sub>2</sub> that are available. We highlight this by expanding our study to include geological and synthetic MoS<sub>2</sub> (Geological B and Synthetic B) from separate sources processed in parallel with Geological A and Synthetic A. The two synthetic samples were produced by different

processes, sulfurization and CVD. The CVD sample underwent a polystyrene mediated transfer process following deposition from the growth substrate onto SiO<sub>2</sub>. As a result of the different fabrication techniques, these two samples inherently exhibit different properties. For example, prior work has shown that sulfurized Mo such as Synthetic A can be vertically aligned while Synthetic B and the geological samples are planar [30]. The two geological samples are obtained from different vendors. The purpose of Experiment 3 is to examine the effect of the same PMMA removal process on the four different materials.

All four samples were spin-coated with PMMA, soaked in acetone, exposed to UV-O<sub>3</sub> for 2 min, and annealed in UHV at 550 °C for 30 min. XPS data, as shown in Fig. 4, was acquired following acetone dissolution, UV-O<sub>3</sub> exposure, and the final annealing step. In the C 1s spectra, it is apparent that carbon removal was more effective in Synthetic B than Synthetic A, and more effective in Geological A than Geological B. Furthermore we note that Synthetic B shows no signs of Mo–O features that are the evidence of Mo–S bond scission in Synthetic A. We note

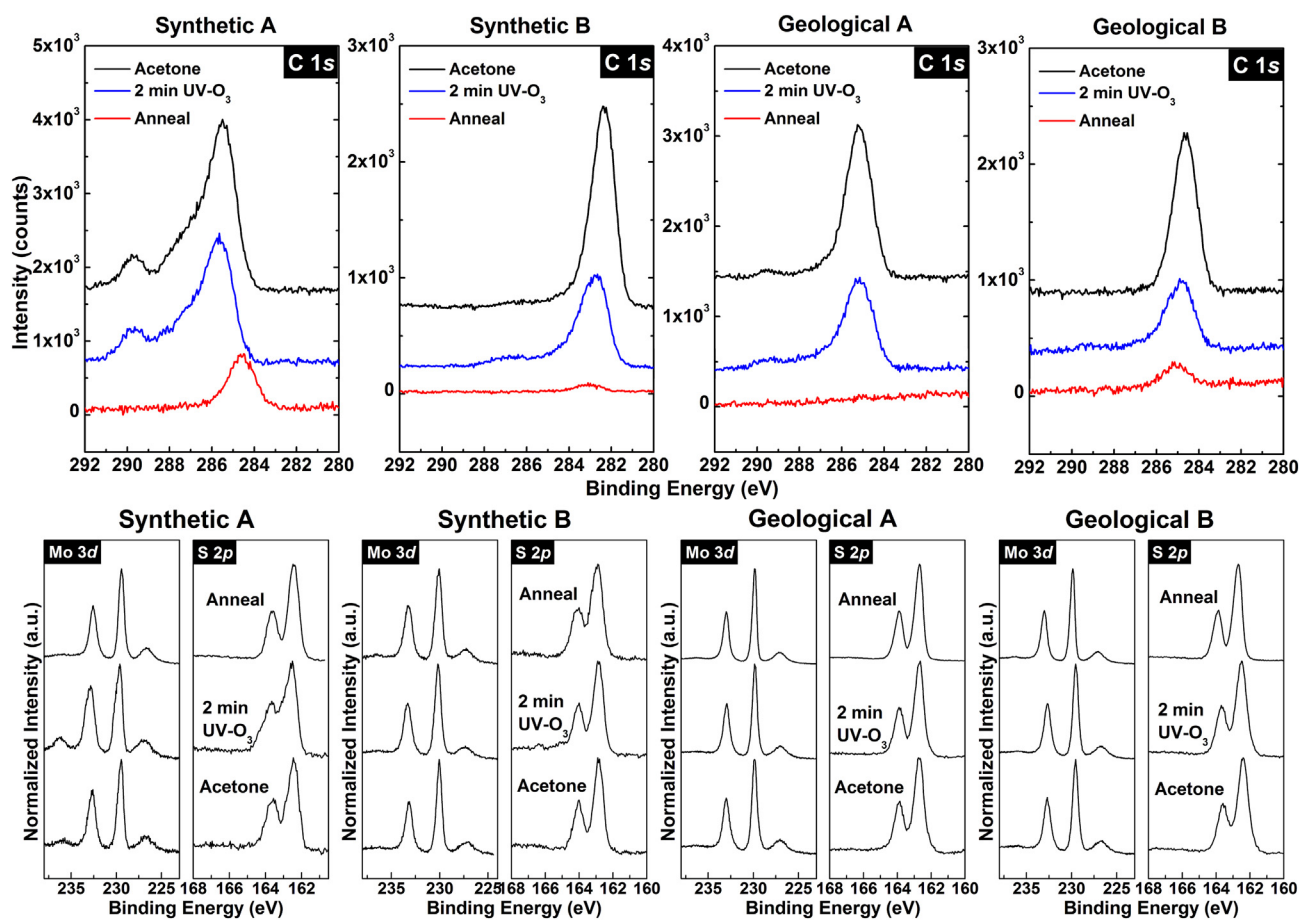


Fig. 4. C 1s, Mo 3d and S 2p spectra acquired after acetone dissolution, after 2 min of UV-O<sub>3</sub> exposure, and after UHV annealing.

that Synthetic B exhibits a significantly lower RMS surface roughness value ( $\approx 450$  pm) than Synthetic A (1.7 nm). Similarly, Geological A exhibits a lower RMS surface roughness (73 pm) than Geological B (120 pm). For a given family of materials (synthetic vs. geological), surface roughness likely plays a role in the efficacy of PMMA removal treatments. While Geological B had a lower RMS surface roughness than Synthetic B, carbon removal was more effective for the synthetic sample. The reason for this is not clear, but it could potentially be due macroscopic defects in the geological sample, such as bunched step edges or other defects, resulting in high sticking coefficient regions that could be missed by AFM but fall within the analysis area of XPS.

We conclude that optimal process parameters for PMMA removal vary depending on the type of MoS<sub>2</sub> material due to differences in surface morphology and material quality. We note that this study examined geological material from two particular vendors and synthetic material fabricated using two specific methods, and our results may not be generalizable for all geological and synthetic samples. This work highlights that not all MoS<sub>2</sub> is created equal, and that optimum PMMA removal process conditions cannot be generalized but are instead dependent on the source of MoS<sub>2</sub>.

## Acknowledgements

The authors acknowledge Dr. Jerrold Floro and Dr. Christopher Duska for aid in acquiring AFM images as well as Costel Constantin from James Madison University for access to AFM for additional AFM images shown in the SI. M. G. S. acknowledges support from the UVA Engineering Distinguished Fellowship. S. K. acknowledges support from the U.S. Department of Commerce, National Institute of Standards and Technology under the financial assistance award 70NANB18H155. P.M.

and A.I. acknowledge support from the Israel Science Foundation, grant numbers 2549/17 and 1784/15. The Phi VersaProbe III XPS used for acquiring the data in Fig. 4 was provided through the NSF-MRI Award #1626201.

## Appendix A. Supplementary data

Supplementary data to this article can be found online at <https://doi.org/10.1016/j.apsusc.2019.01.222>.

## References

- [1] B. Radisavljevic, A. Radenovic, J. Brivio, V. Giacometti, A. Kis, Single-layer MoS<sub>2</sub> transistors, *Nat. Nanotechnol.* 6 (2011) 147–150.
- [2] R. Li, Z. Li, E. Pambou, P. Gutfreund, T.A. Waigh, J.R.P. Webster, J.R. Lu, Determination of PMMA residues on a chemical-vapor-deposited monolayer of graphene by neutron reflection and atomic force microscopy, *Langmuir* 34 (2018) 1827–1833.
- [3] Y.C. Lin, C.C. Lu, C.H. Yeh, C. Jin, K. Suenaga, P.W. Chiu, Graphene annealing: how clean can it be? *Nano Lett.* 12 (2012) 414–419.
- [4] D.S. Macintyre, O. Ignatova, S. Thoms, I.G. Thayne, Resist residues and transistor gate fabrication, *J. Vac. Sci. Technol., B: Microelectron. Nanometer Struct.-Process., Meas., Phenom.* 27 (2009) 2597–2601.
- [5] A. Pirkle, J. Chan, A. Venugopal, D. Hinojos, C.W. Magnuson, S. McDonnell, L. Colombo, E.M. Vogel, R.S. Ruoff, R.M. Wallace, The effect of chemical residues on the physical and electrical properties of chemical vapor deposited graphene transferred to SiO<sub>2</sub>, *Appl. Phys. Lett.* 99 (2011) 122108.
- [6] J. Chan, A. Venugopal, A. Pirkle, S. McDonnell, D. Hinojos, C.W. Magnuson, R.S. Ruoff, L. Colombo, R.M. Wallace, E.M. Vogel, Reducing extrinsic performance-limiting factors in graphene grown by chemical vapor deposition, *ACS Nano* 6 (2012) 3224–3229.
- [7] C. Wei Chen, F. Ren, G.-C. Chi, S.-C. Hung, Y.P. Huang, J. Kim, I.I. Kravchenko, S.J. Pearton, UV ozone treatment for improving contact resistance on graphene, *J. Vac. Sci. Technol., B: Nanotechnol. Microelectron.: Mater., Process., Meas., Phenom.* 30 (2012) 060604.
- [8] J.e.a. Lee, Clean transfer of graphene and its effect on contact resistance, *Appl.*

- Phys. Lett. 103 (2013) 103104.
- [9] W. Li, Y. Liang, D. Yu, L. Peng, K.P. Pernstich, T. Shen, A.R. Hight Walker, G. Cheng, C.A. Hacker, C.A. Richter, Q. Li, D.J. Gundlach, X. Liang, Ultraviolet/ozone treatment to reduce metal-graphene contact resistance, *Appl. Phys. Lett.* 102 (2013) 183110.
- [10] S. McDonnell, B. Brennan, A. Azcatl, N. Lu, H. Dong, C. Buie, J. Kim, C.L. Hinkle, M.J. Kim, R.M. Wallace, HfO<sub>2</sub> on MoS<sub>2</sub> by atomic layer deposition: adsorption mechanisms and thickness scalability, *ACS Nano* 7 (2013) 10354–10361.
- [11] A. Azcatl, S. McDonnell, S.K. C, X. Peng, H. Dong, X. Qin, R. Addou, G.I. Mordi, N. Lu, J. Kim, M.J. Kim, K. Cho, R.M. Wallace, MoS<sub>2</sub> functionalization for ultra-thin atomic layer deposited dielectrics, *Appl. Phys. Lett.* 104 (2014) 111601.
- [12] A. Azcatl, K. Santosh, X. Peng, N. Lu, S. McDonnell, X. Qin, F. De Dios, R. Addou, J. Kim, M.J. Kim, HfO<sub>2</sub> on UV–O<sub>3</sub> exposed transition metal dichalcogenides: interfacial reactions study, *2D Materials* 2 (2015) 014004.
- [13] Q. Van Le, T.P. Nguyen, H.W. Jang, S.Y. Kim, The use of UV/ozone-treated MoS<sub>2</sub> nanosheets for extended air stability in organic photovoltaic cells, *PCCP* 16 (2014) 13123–13128.
- [14] X. Yang, W. Fu, W. Liu, J. Hong, Y. Cai, C. Jin, M. Xu, H. Wang, D. Yang, H. Chen, Engineering crystalline structures of two-dimensional MoS<sub>2</sub> sheets for high-performance organic solar cells, *J. Mater. Chem. A* 2 (2014) 7727–7733.
- [15] S. Park, S.Y. Kim, Y. Choi, M. Kim, H. Shin, J. Kim, W. Choi, Interface properties of atomic-layer-deposited Al<sub>2</sub>O<sub>3</sub> thin films on ultraviolet/ozone-treated multilayer MoS<sub>2</sub> crystals, *ACS Appl. Mater. Interfaces* 8 (2016) 11189–11193.
- [16] S. Kurabayashi, K. Nagashio, Tolerance to UV-O<sub>3</sub> exposure of CVD and mechanically exfoliated MoS<sub>2</sub> & fabrication of top-gated CVD MoS<sub>2</sub> FETs, 2015 International Conference on Solid State Devices and Materials, 2015.
- [17] A. Tarasov, P.M. Campbell, M.Y. Tsai, Z.R. Hesabi, J. Feirer, S. Graham, W.J. Ready, E.M. Vogel, Highly uniform Trilayer molybdenum disulfide for wafer-scale device fabrication, *Adv. Funct. Mater.* 24 (2014) 6389–6400.
- [18] Y. Liu, R. Ghosh, D. Wu, A. Ismach, R. Ruoff, K. Lai, Mesoscale imperfections in MoS<sub>2</sub> atomic layers grown by a vapor transport technique, *Nano Lett.* 14 (2014) 4682–4686.
- [19] A. Gurarslan, Y. Yu, L. Su, Y. Yu, F. Suarez, S. Yao, Y. Zhu, M. Ozturk, Y. Zhang, L. Cao, Surface-energy-assisted perfect transfer of centimeter-scale monolayer and few-layer MoS<sub>2</sub> films onto arbitrary substrates, *ACS Nano* 8 (2014) 11522–11528.
- [20] SPI, <https://www.2spi.com/>.
- [21] Ward's, <https://www.wardsci.com/store/>.
- [22] K.M. Freedy, P.M. Litwin, S.J. McDonnell, (Invited) in-Vacuo studies of transition metal dichalcogenide synthesis and layered material integration, *ECS Trans.* 77 (2017) 11–25.
- [23] T.L. Barr, S. Seal, Nature of the use of adventitious carbon as a binding energy standard, *J. Vac. Sci. Technol. A* 13 (1995) 1239–1246.
- [24] J. Quereda, A. Castellanos-Gomez, N. Agrait, G. Rubio-Bollinger, Single-layer MoS<sub>2</sub> roughness and sliding friction quenching by interaction with atomically flat substrates, *Appl. Phys. Lett.* 105 (2014) 053111.
- [25] G. Beamson, A. Bunn, D. Briggs, High-resolution monochromated XPS of poly (methyl methacrylate) thin films on a conducting substrate, *Surf. Interface Anal.* 17 (1991) 105–115.
- [26] D. Briggs, G. Beamson, Primary and secondary oxygen-induced C1s binding energy shifts in x-ray photoelectron spectroscopy of polymers, *Anal. Chem.* 64 (1992) 1729–1736.
- [27] S. McDonnell, R. Addou, C. Buie, R.M. Wallace, C.L. Hinkle, Defect-dominated doping and contact resistance in MoS<sub>2</sub>, *ACS Nano* 8 (2014) 2880–2888.
- [28] N.M.D. Brown, N. Cui, A. McKinley, An XPS study of the surface modification of natural MoS<sub>2</sub> following treatment in an RF-oxygen plasma, *Appl. Surf. Sci.* 134 (1998) 11–21.
- [29] M.R. Laskar, L. Ma, S. Kannappan, P. Sung Park, S. Krishnamoorthy, D.N. Nath, W. Lu, Y. Wu, S. Rajan, Large area single crystal (0001) oriented MoS<sub>2</sub>, *Appl. Phys. Lett.* 102 (2013) 252108.
- [30] Y. Jung, J. Shen, Y. Liu, J.M. Woods, Y. Sun, J.J. Cha, Metal seed layer thickness-induced transition from vertical to horizontal growth of MoS<sub>2</sub> and WS<sub>2</sub>, *Nano Lett.* 14 (2014) 6842–6849.